HIV requires multiple gp120 molecules for CD4-mediated infection

Scott P. Layne*, Michael J. Merges†, Micah Dembo*, John L. Spouge‡ & Peter L. Nara†

* Theoretical Division, Los Alamos National Laboratory, Los Alamos, New Mexico 87545, USA
† Virus Biology Section, Laboratory of Tumor Cell Biology, NCI-FCRF, Frederick, Maryland 21701, USA
‡ National Center for Biotechnology Information, National Library of Medicine, Bethesda, Maryland 20894, USA

BINDING of glycoprotein gp120 to the T cell-surface receptor CD4 is a crucial step in CD4-dependent infection of a target cell by the human immunodeficiency virus (HIV)[1–5]. Blocking some or all gp120 molecules on the viral surface should therefore inhibit infection. Consequently, competitive receptor inhibitors, such as soluble synthetic CD4 (sCD4), synthetic CD4 peptides and immunoglobulins, have been investigated *in vitro*[6–17] and *in vivo*[18–20], but little is known about the molecular mechanisms of these inhibitors. We have now quantitatively examined blocking by soluble CD4 in the hope of gaining insight into the complex process of viral binding, adsorption and penetration. At low sCD4 concentrations, the inhibition in three HIV strains is proportional to the binding of gp120. The biological association constant (gp120-sCD4 K_{assoc}) for HIV-2_{NIHZ} is $(8.5 \pm 0.5) \times 10^7$ M^{-1}, whereas K_{assoc} for HIV-1_{HXB3} (1.4 ± 0.2) and HIV-1_{MN} $(1.7 \pm 0.1) \times 10^9$ M^{-1} are 15–20-fold larger. For all three viral strains, the biological K_{assoc} from infectivity assays is comparable to the chemical K_{assoc}. The inhibitory action of sCD4 at high concentrations, however, is not fully explained by simple proportionality with the binding to gp120. Positive synergy in blocking of infection occurs after about half the viral gp120s molecules are occupied, and is identical for all three viral strains, despite the large differences in K_{assoc}. Our method of measuring the viral–cell receptor K_{assoc} directly from infectivity assays is applicable to immunoglobulins, to other viruses and to assays using primary or transformed cell lines.

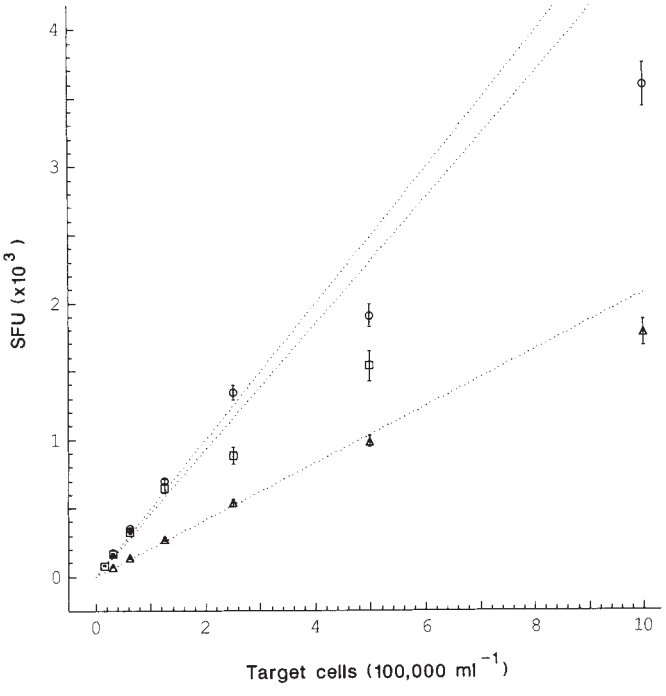

A quantitative infectivity assay requires the number of infectious events to be linear (unsaturated) in the target cell concentration[21,22]. Figure 1 shows results for six concentrations of CEM-SS cells[23,24]. Results were linear at lower cell concentrations and showed only minor assay saturation at higher concentrations. The multiplicity of infection in all assays was less than 0.025 (see Fig. 1, methods).

To distinguish among the possible mechanisms by which sCD4 blocks gp120-mediated infection, we previously analysed a kinetic model of the initial events of infection[21,22], in which each gp120 monomer within an oligomer is functionally independent and equivalent. This neutral hypothesis predicts that for an unsaturated assay, a plot of inverse infection (1/SFU, where SFU are syncytial-forming units) versus sCD4 concentration should be a straight line. That is, inhibition is proportional to binding. Dividing the slope of an inverse infection plot by its intercept gives the gp120–sCD4 K_{assoc}. Upward curvature in the inverse infection plot indicates positive synergy between gp120 molecules as they promote infection or between sCD4

FIG. 1 Examining the linearity of infectivity assays. To compare one assay with another, they must scale linearly with target cell concentration, because saturated assays make blockers seem ineffective[21,22]. The graphs for HIV-1_{HXB3} (○), HIV-1_{MN} (□) and HIV-2_{NIHZ} (△) show SFU plotted against target cell concentration. For each viral strain, assays were conducted at six target-cell and seven sCD4 concentrations (see Table 1). All results are the mean of eight microtitre wells (bars show ± 1 s.d.). Results without sCD4 are shown; similar results were obtained when sCD4 was added to the assays. The dotted lines are weighted least-squares fits. At all sCD4 concentrations, correlation coefficients were ≥0.89 for HIV-1_{HXB3}, ≥0.97 for HIV-1_{MN} and ≥0.98 for HIV-2_{NIHZ}, substantiating that the infectivity assays were linear at the lower, more heavily weighted, cell concentrations.

METHODS. The HIV-1 and HIV-2 stocks were acutely collected from H9 cells to optimize infectivity[23]. HIV-1 *in vivo* is a mixture of closely related viral subpopulations with minor envelope variations[31]. To address the influence of envelope microheterogeneity on infectivity[32–34], we studied both a molecularly cloned viral stock (HIV-1_{HXB3}) and two uncloned viral stocks (HIV-1_{MN} and -2_{NIHZ})[26]. HIV-1_{MN} was selected because of its dominance in recent seroprevalence surveys[35]. In typical viral stocks, gp120 is not only present on virions as oligomers[36] but also exists as soluble gp120 monomers[37]. Thus, soluble gp120 may cause artefacts if it competes significantly with viral-associated gp120 for sCD4 or cell-surface CD4. In the present study, radioimmunoassay[38] was used to measure the total gp120 (soluble plus viral-associated) in all HIV stocks tested. The total gp120 in the viral inocula was 1×10^{-10}, 6×10^{-11} and 3×10^{-12} M for HIV-1_{HXB3}, HIV-1_{MN} and HIV-2_{NIHZ}, respectively. These concentrations of total gp120 were, in the worst case, more than sevenfold smaller than $1/K_{assoc}$. Hence, the association of soluble gp120 with sCD4 or cell-surface CD4 was negligible in all viral stocks[23] used in this study. Infectious events were quantified by a modified version of the syncytium-forming assay[23,24]. The modifications minimized artefacts associated with high cell concentrations in conjunction with sCD4 in the assay. Before the assay, CEM-SS cells were grown at low concentrations ($<5 \times 10^5$ ml^{-1}) to assure logarithmic growth. On the day of an assay, cells were suspended in fresh medium at densities of 4.5×10^5 and 2×10^6 ml^{-1} to serve as 'indicator' and 'target' cell stocks, respectively. Target cells (0.5 ml) were then transferred to culture tubes containing six different volumes of fresh medium and seven different sCD4 concentrations (total of 42 tubes). The final target-cell densities in the culture tubes were 1×10^6, 5×10^5, 2.5×10^5, 1.25×10^5, 6.25×10^4 and 3.13×10^4 ml^{-1}. The respective reaction volumes were 1, 2, 4, 8, 16 and 32 ml. Identical multiplicities of infection (in graded volumes of viral stock) were added to each tube, resulting in a constant viral inoculum to reaction volume of 10%. To assure uniform mixing, culture tubes were rolled (~10 turns per min) during the 2-hour infection period. Next, the infected target cells were washed three times (centrifugation for 5 min, 200*g*, followed by suspension in 40 ml fresh medium and another centrifugation) and suspended in fresh medium at 5×10^4 cells ml^{-1}. This thorough washing of sCD4 from the target cells prevented subsequent inhibition of syncytium formation in the monolayer of target and indicator cells (two washes removed all sCD4, data not shown). Cell monolayers were prepared by adding 4.5×10^4 indicator cells (0.1 ml) and 5×10^3 target cells (0.1 ml) to flat-bottomed microtitre wells (indicator:target cell ratio of 9:1). A total of eight wells were plated per sCD4 and target-cell concentration. Syncytia (representing the infection of individual target cells by cell-free virus) were counted on days three (HIV-2) or five (HIV-1) after infection. The above description applies to HIV-1_{HXB3} assays (an indicator to target-cell ratio of 90:1 gave identical results to the 9:1 ratio used here, data not shown). For HIV-1_{MN} assays, target-cell stocks were prepared at 1×10^6 cells ml^{-1} and target-cell densities in the culture tubes were twofold smaller. For HIV-2_{NIHZ} assays, indicator-cell stocks were prepared at 6.5×10^5 cells ml^{-1}; infected target-cells were washed and suspended at 1×10^5 cells ml^{-1} (indicator:target-cell ratio of 6.5:1). For assays with reaction volumes of 1, 2, 4, 8, 16 and 32 ml, the comparative number of SFU were calculated by multiplying actual number of SFU in each well by 32, 16, 8, 4, 2 and 1, respectively. Minimizing $f(a,b) = \Sigma\{[y_i - (ax_i + b)]/\sigma_i\}^2$ gives a weighted least-squares linear fit to the data (y_i is the mean value of SFU at the ith sCD4 concentration, σ_i is the s.d. of SFU, and x_i is the blocker concentration at the ith data point). Terms in the correlation coefficient[39] were weighted by $1/\sigma_i^2$. A weighted correlation coefficient = 1 means that the least-squares line fits the data perfectly.

molecules as they bind to and block gp120. Downward curvature indicates corresponding negative synergy.

Figure 2 shows the inverse infection plot for HIV-2_{NIHZ} at 1×10^6 target cells per ml. The plot curves progressively upward at higher sCD4 concentrations, indicating positive synergy in sCD4 blocking. Nevertheless, the data are linear at lower blocker concentrations and allow the determination of K_{assoc}. For example, the straight line in Fig. 2 gives a K_{assoc} of about 8.56×10^7 M^{-1} and the five other target cell concentrations gave comparable K_{assoc} (Table 1). K_{assoc} was also independent of the target cell concentration for the two strains of HIV-1 studied.

A chemical association constant for gp120-sCD4 binding cannot be presumed to measure a biological K_{assoc}, but it can be compared with the biological K_{assoc} as shown in Table 1. Despite a 20-fold difference in K_{assoc} between the viral types, the chemical measurements agree quite closely with our own. This difference agrees with reports of reduced blocking activity by sCD4 for HIV-2 in comparison with HIV-1[12,25,41]. Thus, the initial slope of the inverse infection plot[21,22] demonstrates that the biological activity of sCD4 (at low concentrations) is primarily due to reversible blocking of viral gp120 cell-surface CD4 interactions.

To analyse the synergistic blocking activity at higher concentrations, we normalized the inverse infection plot as follows. The inverse infection is divided by its control—inverse infection without blocker. The concentration of sCD4 is multiplied by K_{assoc}, giving a numerical value of one to the sCD4 concentration at which half the gp120 molecules are blocked (see Fig. 3). Surprisingly, after normalization, the shape of the inverse infection plot is independent of the target cell concentration, the value of K_{assoc}, and the viral type.

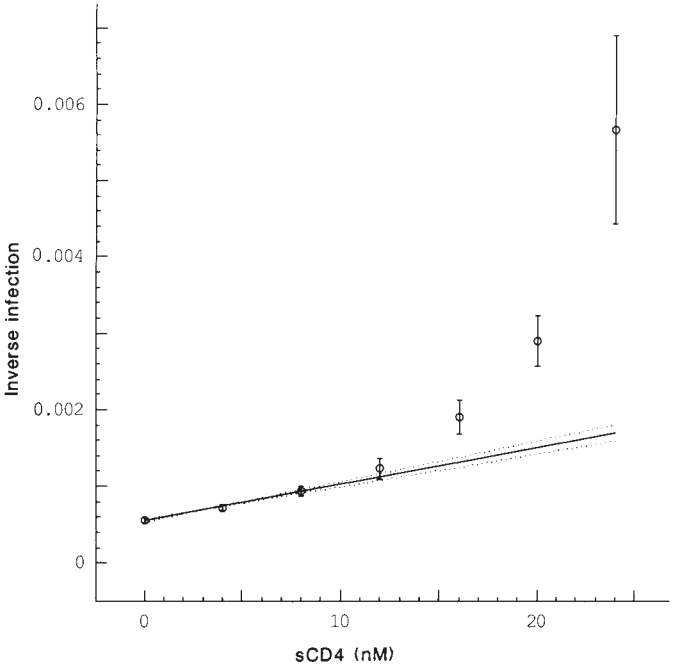

FIG. 2 Calculating the gp120-sCD4 K_{assoc} from infectivity assays. When infectivity assays scale linearly with target cell concentration, a plot of inverse infection (1/SFU) versus sCD4 concentration should yield a straight line with slope/intercept $\approx K_{assoc}$ (refs 21, 22). An example of this inverse infection plot is illustrated for HIV-2_{NIHZ}, when target cell concentration is 1×10^6 cells ml^{-1}. The solid line is a weighted least-squares fit to the data (bars show mean ± 1 s.d.) at sCD4 concentrations of 0, 4, 8 and 12 nM. The fit has weighted correlation coefficient of ~0.99, slope of $\sim 4.75 \times 10^4$ M^{-1}, and intercept of $\sim 5.56 \times 10^4$, giving $K_{assoc} \approx 8.56 \times 10^7$ M^{-1} (y_i is the mean value of 1/SFU, see Fig. 1 methods). The dotted lines are the 95% confidence limits for the fit. Both limits were calculated by a standard bootstrap method[40] and, in this example, give $7.47 \times 10^7 \leq K_{assoc} \leq 8.86 \times 10^7$ M^{-1}. For the three viral strains, we calculated K_{assoc} from the lower four sCD4 concentrations in Table 1. The weighted correlation coefficients for all the fits are ≥0.85 for HIV-1_{HXB3}, ≥0.98 for HIV-1_{MN} and ≥0.99 for HIV-2_{NIHZ}, indicating nearly complete explanations of the data at the lower sCD4 concentrations.

TABLE 1 Summary of the gp120-sCD4 K_{assoc}

Viral strain	Target cells (ml^{-1})	K_{assoc} ± 1 s.d. (M^{-1})	Mean K_{assoc} ± 1 s.d. (M^{-1})
HIV-1_{HXB3}	3.13×10^4	$(1.38 \pm 0.17) \times 10^9$	
	6.25×10^4	$(1.34 \pm 0.15) \times 10^9$	
	1.25×10^5	$(1.34 \pm 0.17) \times 10^9$	
	2.50×10^5	$(1.30 \pm 0.18) \times 10^9$	
	5.00×10^5	$(1.16 \pm 0.15) \times 10^9$	
	1.00×10^6	$(1.90 \pm 0.39) \times 10^9$	
			$(1.4 \pm 0.20) \times 10^9$
HIV-1_{MN}	1.56×10^4	$(1.46 \pm 0.10) \times 10^9$	
	3.13×10^4	$(1.82 \pm 0.14) \times 10^9$	
	6.25×10^4	$(1.84 \pm 0.14) \times 10^9$	
	1.25×10^5	$(1.65 \pm 0.09) \times 10^9$	
	2.50×10^5	$(1.89 \pm 0.14) \times 10^9$	
	5.00×10^5	$(1.45 \pm 0.15) \times 10^9$	
			$(1.7 \pm 0.13) \times 10^9$
HIV-2_{NIHZ}	3.13×10^4	$(9.46 \pm 0.64) \times 10^7$	
	6.25×10^4	$(9.16 \pm 0.42) \times 10^7$	
	1.25×10^5	$(8.89 \pm 0.76) \times 10^7$	
	2.50×10^5	$(7.67 \pm 0.38) \times 10^7$	
	5.00×10^5	$(7.48 \pm 0.42) \times 10^7$	
	1.00×10^6	$(8.56 \pm 0.64) \times 10^7$	
			$(8.5 \pm 0.54) \times 10^7$

For each viral strain and target cell concentration, target cells were infected at seven sCD4 concentrations. For HIV-1_{HXB3}, sCD4 concentrations were: 0, 4.0×10^{-10}, 8.0×10^{-10}, 1.2×10^{-9}, 1.6×10^{-9}, 2.0×10^{-9}, 2.4×10^{-9} M. For HIV-1_{MN}, sCD4 concentrations were 0, 2.0×10^{-10}, 4.0×10^{-10}, 6.0×10^{-10}, 8.0×10^{-10}, 1.0×10^{-9}, 1.2×10^{-9} M. For HIV-2_{NIHZ}, sCD4 concentrations were 0, 4.0×10^{-9}, 8.0×10^{-9}, 1.2×10^{-8}, 1.6×10^{-8}, 2.0×10^{-8}, 2.4×10^{-8} M. Using the same soluble CD4 (CD4T) as our study and Scatchard analysis, methods based on the chemical K_{assoc} for HIV-1_{IIIB} was reported as $(1.19 \pm 0.14) \times 10^9$ M^{-1} (ref. 7). Using enzyme-linked immunosorbent assay (ELISA), the chemical K_{assoc} for HIV-1_{IIIB} and HIV-2_{ROD} was $(8.0 \pm 4.8) \times 10^8$ and $(2.2 \pm 1.1) \times 10^7$ M^{-1}, respectively[41]. HIV-1_{IIIB} and HIV-1_{HXB3} differ by 0.5% in their gp120 nucleotide sequence; HIV-2_{ROD} and HIV-2_{NIHZ} differ by 12% (ref. 26). On the basis of nucleotide similarity, the HIV-1 strains permit the most direct comparison between biological and chemical K_{assoc}.

When sCD4 blocks less than half of the gp120 molecules on virus optimized for infectivity[23] ($\beta < 1$, so $1/(1+\beta) > 1/2$, where $\beta = [\text{sCD4}] \times K_{assoc}$), the normalized infection plot (Fig. 3) is linear, indicating each gp120 molecule independently and equivalently contributes to infection[21,22]. But when more than half the gp120 molecules are blocked ($\beta > 1$), the assumption of equivalent and independent gp120 monomers cannot explain all the blocking of infection *in vitro*.

Some explanations can be excluded immediately. Because the cloned viral stock (HIV-1_{HXB3}) gave the same results as the two uncloned viral stocks (HIV-1_{MN} and -2_{NIHZ})[26], the cooperativity is probably not caused by heterogeneous gp120s with differing K_{assoc}. Assay artefacts causing spurious cooperativity, such as interference by soluble gp120, have been ruled out (see legend to Fig. 1). Soluble CD4 might have enhanced the shedding or direct inactivation of viral gp120, but a simple extension of our model[21,22] shows the slope of the inverse infection plot would simply overestimate K_{assoc} and would not produce the upward curvature shown in Fig. 3.

One possibility is that a single gp120–CD4 interaction initiates viral binding, whereas viral adsorption and penetration require subsequent recruitment of additional gp120–CD4 interactions. Recruitment accounts for cooperativity and is consistent with experiments using sCD4 and immunoglobulins to inhibit infection after initial binding[12,17,27]. The recruitment hypothesis predicts that aged viral stocks (with virions that have shed most of

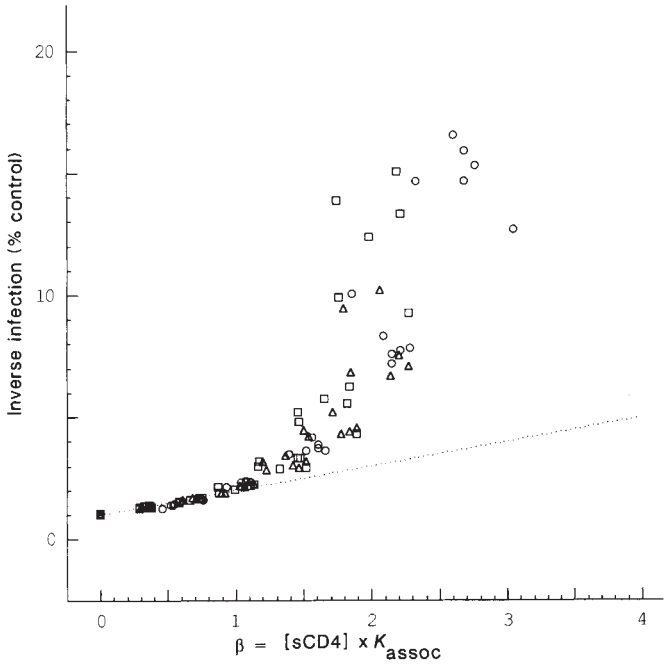

FIG. 3 Analysing the cooperative blocking activity of sCD4. Dividing inverse infection (Fig. 2) by its control (inverse infection without blocker) and multiplying sCD4 concentrations by the apparent K_{assoc} yields a normalized plot of inverse infection. Each normalization used the K_{assoc} calculated from the same target cell concentration (Table 1). The fraction of gpl20 molecules that are either free or blocked by a particular concentration of sCD4 is given by $1/(1+\beta)$ and $\beta/(1+\beta)$ respectively, where $\beta = [sCD4] \times K_{assoc}$. Results at all six target cell concentrations for HIV-1_{HXB3} (○), HIV-1_{MN} (□) and HIV-2_{NIHZ} (△). The dotted line represents blocking based on independent and equivalent gp120s (refs 21, 22). When less than half the gp120 molecules are blocked, the points lie on the dotted line. When half the gp120 molecules are blocked, deviations indicating sCD4 blocking synergy begin to occur. The synergies are identical for each viral strain.

their gp120) will be more easily blocked, thus enhancing the cooperativity in Fig. 3. Another explanation is that there are allosteric interactions between gp120s on the viral coat. This, in contrast to the recruitment model, predicts that the cooperativity of aged viral stocks will be unchanged or even decreased.

The upward curvature of the inverse infection plot is apparent only after half of the gp120 binding sites are blocked. Thus, the HIV envelope is covered by a highly redundant number of gp120 molecules which act independently at low sCD4 concentrations. Unlike HIV, viruses such as polio and influenza are covered by interacting (metastable) capsid polypeptide subunits and interacting glycoprotein subunits, respectively, which present relatively few critical neutralization sites. When a fraction of these sites are blocked by neutralizing antibodies, a non-local transition in subunit orientation is induced that inactivates the virus[28–30]. This property may contribute to the humoral efficacy of vaccines against polio and influenza. Neutralizing HIV, however, seems to be fundamentally different. □

Received 19 December 1989; accepted 17 May 1990.

1. Dalgleish, A. G. *et al. Nature* **312,** 763–767 (1984).
2. Klatzmann, D. *et al. Nature* **312,** 767–768 (1984).
3. McDougal, J. S. *et al. Science* **231,** 382–385 (1986).
4. Kowalski, M. *et al. Science* **237,** 1351–1355 (1987).
5. Bedinger, P. *et al. Nature* **334,** 162–165 (1988).
6. Lasky, L. A. *et al. Cell* **50,** 975–985 (1987).
7. Smith, D. H. *et al. Science* **238,** 1704–1707 (1987).
8. Fisher, R. A. *et al. Nature* **331,** 76–78 (1988).
9. Hussey, R. E. *et al. Nature* **331,** 78–81 (1988).
10. Deen, K. C. *et al. Nature* **331,** 82–84 (1988).
11. Traunecker, A., Lüke, W. & Karjalainen, K. *Nature* **331,** 84–86 (1988).
12. Clapham, P. R. *et al. Nature* **337,** 368–370 (1989).
13. Capon, D. J. *et al. Nature* **337,** 525–531 (1989).
14. Traunecker, A., Schneider, J., Kiefer, H. & Karjalainen, K. *Nature* **339,** 68–70 (1989).
15. Nara, P. L., Hwang, K. M., Rausch, D. M., Lifson, J. D. & Eiden, L. E. *Proc. natn. Acad. Sci. U.S.A.* **86,** 7139–7143 (1989).
16. Sun, N.-C. *et al. J. Virology* **63,** 3579–3585 (1989).
17. Byrn, R. A. *et al. J. Virology* **63,** 4370–4375 (1989).
18. Watanabe, M. *et al. Nature* **337,** 267–270 (1989).
19. Schooley, R. T. *et al. Ann. intern. Med.* **112,** 247–253 (1990).
20. Kahn, J. O. *et al. Ann. intern. Med.* **112,** 254–261 (1990).
21. Layne, S. P., Spouge, J. L. & Dembo, M. *Proc. natn. Acad. Sci. U.S.A.* **86,** 4644–4648 (1989).
22. Spouge, J. L., Layne, S. P. & Dembo, M. *Bull. math. Biol.* **51,** 715–730 (1989).
23. Nara, P. L. *et al. AIDS Res. hum. Retroviruses* **3,** 283–302 (1987).
24. Nara, P. L. & Fischinger, P. J. *Nature* **332,** 469–470 (1988).
25. Sweet, R. *et al. Fifth Int. Conf. AIDS Abstr.* W.C.O. 12 (1989).
26. Myers, G. *et al. Human Retroviruses and AIDS* Section III, 9–12 (Los Alamos National Laboratory, New Mexico, 1990).
27. Nara, P. L. in *Vaccines 89* (eds Lerner, R. A., Ginsberg, H., Chanock, R. M. & Brown, F.) 137–144 (Cold Spring Harbor Laboratory, New York, 1989).
28. Icenogle, J. *et al. Virology* **127,** 412–425 (1983).
29. Emini, E. A., Ostapchuk, P. & Wimmer, E. *J. Virology* **48,** 547–550 (1983).
30. Taylor, H. P., Armstrong, S. J. & Dimmock, N. J. Virology **159,** 288–298 (1987).
31. Goudsmit, J. *et al. Proc. UCLA Symposia* (in the press).
32. Looney, D. J. *et al. Science* **241,** 357–359 (1988).
33. Saag, M. S. *et al. Nature* **334,** 440–444 (1989).
34. Cordonnier, A., Montagnier, L. & Emerman, M. *Nature* **340,** 571–574 (1989).
35. Zwart, G. *et al. Lancet* **i,** 474 (1990).
36. Özel, M., Pauli, G. & Gelderblom, H. R. *Arch. Virology* **100,** 255–266 (1988).
37. Earl, P. L., Doms, R. W. & Moss, B. *Proc. natn. Acad. Sci. U.S.A.* **87,** 648–652 (1990).
38. Pyle, S. W. *et al. AIDS Res. Hum. Retroviruses* **3,** 387–400 (1987).
39. Kendall, M. & Stuart, A. *The Advanced Theory of Statistics* Vol. 2 (Griffin, London, 1979).
40. Efron, B. & Tibshirani, R. *Stat. Sci.* **1,** 54–77 (1986).
41. Moore, J. P. *AIDS* **4,** 297–305 (1990).

ACKNOWLEDGEMENTS. We thank Drs R. C. Gallo, F. Wong-Staal, M. Popovic and D. Zagury for providing HIV-1_{HXB3}, HIV-1_{MN} and HIV-2_{NIHZ}, and D. J. Capon and R. Ward (Genentech) for sCD4. This work was financially supported by the US Army Medical Research and Development Command, US Department of Energy, and the NIH.

Additional deletion in sex-determining region of human Y chromosome resolves paradox of X,t(Y;22) female

David C. Page*, Elizabeth M. C. Fisher*, Barbara McGillivray† & Laura G. Brown*

* Whitehead Institute for Biomedical Research, Nine Cambridge Center, and Department of Biology, Massachusetts Institute of Technology, Cambridge, Massachusetts 02142, USA
† University of British Columbia Clinical Genetics Unit, Vancouver, British Columbia V6H 3N1, Canada

WHETHER a human embryo develops as a male or a female is determined by the presence of the Y chromosome[1,2]. The sex-determining function lies entirely in interval 1A, inasmuch as most XX individuals with descended testes and normal male external genitalia carry this small region of the Y chromosome[3]. We have localized an essential part of the sex-determining function to a portion of interval 1A, on the basis of the discovery of a female with a reciprocal Y;22 translocation and part of 1A deleted at the translocation breakpoint[3]. Recently, a paradox has arisen with the report[4] of four partially masculinized XX individuals who carry only a portion of interval 1A—a portion that does not overlap the deletion in the X,t(Y;22) female. These recent findings imply that the sex-determining function lies in the portion of 1A present in the four XX intersexes and not in the portion deleted in the X,t(Y;22) female. To explain the X,t(Y;22) individual, it was proposed that she was female because of a chromosomal position effect[4] or delayed development of the gonadal soma[5]. Here we report that the X,t(Y;22) female has a deletion of a second portion of interval 1A—a portion corresponding closely to that present[4] in the XX intersexes. This resolves the apparent contradiction. Nonetheless, phenotype–genotype correlations suggest that two or more genetic elements in interval 1A may contribute to the sex-determining function of the Y chromosome. The X,t(Y;22) female